Journal of the Brazilian Society of Mechanical Sciences and Engineering (2022) 44:374
https://doi.org/10.1007/s40430-022-03674-w

TECHNICAL PAPER

Metamodeling-assisted probabilistic first ply failure analysis of laminated composite plates—RS-HDMR- and GPR-based approach

Subrata Kushari[1] · Kritesh Kumar Gupta[1] · Vaishali[1] · Sudip Dey[1]

Received: 18 February 2022 / Accepted: 7 July 2022 / Published online: 2 August 2022

Abstract
In structural applications, laminated composites are typically the best choice for providing a high strength-to-weight ratio. The composite laminates, on the other hand, are susceptible to the first ply failure (FPF), which can result in delamination, matrix cracking, and fiber breaking. As a result, it is critical to map the FPF of laminated composites against the uncertainty in material properties. In this paper, we presented a framework based on coupled statistical modeling and failure criteria to perform sensitivity analysis corresponding to the FPF of laminated composites. The practically relevant randomness in material properties (elastic modulus, shear modulus, Poisson's ratio, and mass density) is enforced by utilizing the Monte Carlo random sampling method. The FPF of a laminated composite subjected to random material properties is evaluated using five failure criteria: maximum strain, maximum stress, Tsai-Hill, Tsai-Wu, and Hoffman. Such a random sampling-based dataset is used to train and validate the random sampling high dimensional model representation (RS-HDMR) metamodel and Gaussian process regression (GPR) model. To ensure sound generalization capabilities, the models are rigorously cross-validated. With sufficient confidence in the constructed models, the models are further utilized to perform the variance-based sensitivity analysis. It is worth mentioning that observations from both models in terms of parameters with the highest sensitivity (for the first-order polynomial function) are comparable. The RS-HDMR metamodel is further used to perform the second-order polynomial function-based sensitivity analysis, wherein the sensitivity index for the most sensitive parameter is observed to be very low when compared with the observations of first-order polynomial function-based sensitivity analysis. The numerically quantifiable outcomes of the present study will serve its purpose in the bottom-up design of the laminated composites.

Technical Editor: Andre T. Beck.

✉ Kritesh Kumar Gupta
kritesh_rs@mech.nits.ac.in

[1] Department of Mechanical Engineering, National Institute of Technology Silchar, Silchar, India

Graphical Abstract

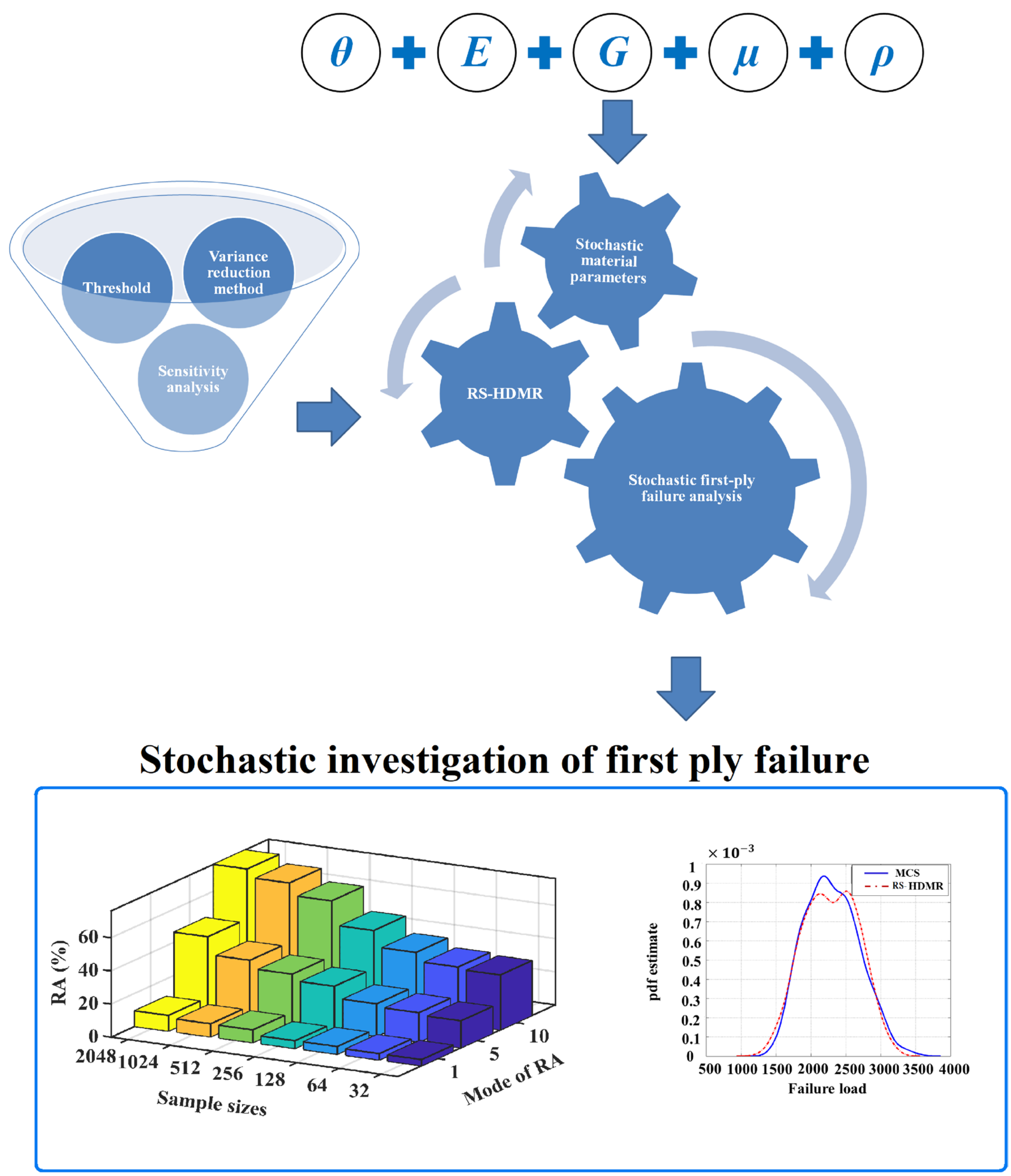

Keywords First-ply failure · Stochastic · RS-HDMR · GPR · MCS · Variance-based sensitivity analysis

List of symbols

Π	Total potential energy
U	Total strain energy
V	Total work potential due to external forces
$d\phi$	Incremental displacement
q_z	Load intensity (transverse) of laminate
σ	Stress component
ε	Strain vector
$\delta_x, \delta_y, \delta_z$	Displacement terms
θ_x and θ_y	Rotational components at matrix level

ϕ_x and ϕ_y	Rotational components at the nodal level
k_x, k_y and k_{xy}	The curvature of the reference plane
$\tilde{D}$	Displacement resultant
$\tilde{M}$	Moment resultant
$\tilde{T}$	Transverse shear resultant
[A], [B] and [D]	Extensional, flexural extensional, and flexural stiffness matrix
ψ_j^e	Shape function
u	Displacement
ε_x^0, ε_x^0 and γ_{xy}^0	Strain in the reference plane
ξ and η	Axis of the principal coordinate system
k	Stiffness
ς and φ	Local natural coordinates of the element
$P_0, P_1 \ldots P_7$	Generalized degree of freedom (DOF)
$\bar{s}_i$	Shape function of node
[J]	Jacobian matrix
θ_x and θ_y	The rotational component in x and y directions in each node
u_0, v_0 and w_0	Displacement variables for laminated plate
θ	Ply-orientation angle
E_1	Longitudinal elastic modulus of elasticity
E_2	Transverse elastic modulus of elasticity
G_{12}	Shear modulus along a longitudinal direction (first and second plane)
G_{13}	Shear modulus along the transverse direction (first and third plane)
G_{23}	Shear modulus in the second and third plane
ρ	Mass density
μ	Poisson's ratio
N_s	Sample size
y_i	Actual model
$\overset{\vartriangle}{y}_i$	Predicted model
$\bar{y}_i$	Mean data
$J(x)_{\text{actual}}$	Actual response of the model
$J(x)_{\text{predicted}}$	Predicted response model
V_t	Total variance
V_P	Partial variance
S_a	Global sensitivity index

1 Introduction

The failure of composite structures has alarmed significant attention and challenges among the research community. It is difficult to construct a reliable and robust composite structure unless the failure of such structure is properly addressed. Due to inherent anisotropy in composition and structure, the uncertainty in its structural behavior is unavoidable [1]. It leads to the variability in modes of failure of such structures. The material parameters such as elastic modulus, density, Poisson's ratio, and geometric parameters such as length, orientation, and thickness are critical in identifying system uncertainty in structural analysis. The literature suggests several approaches for identifying system uncertainty, including the probabilistic approach [2–5], the non-probabilistic approach [6–8], the stochastic finite element method [9, 10], the perturbation method [11, 12], and meta-modeling [13–17]. The means of uncertainty quantification reported in the past are limited in corroborating with the recent advancements in computational technology; hence, novel techniques are developed by the academic and industrial research community. Kam and Jan [18] are among the pioneers in modeling first-ply failure, wherein they utilized the finite element (FE) method along with the layer-wise linear displacement theory to formulate the FPF of a multilayered composite plate. In another study, Reddy and Pandey [19] reported the deterministic approach to design the failure of the system by utilizing tensor-based failure criteria. A few notable previous studies investigated the probabilistic approach used in the first-ply failure (FPF) of the laminated composite [20–24], using the crude Monte Carlo simulation (MCS) [25], stochastic FE method, and perturbation method.

The concise literature review revealed that implementing computationally efficient metamodels for large-scale characterization of FPF of laminated composites is not extensively explored. In their recent studies, only a few groups used metamodeling for FPF analysis of different structures [26, 27]. Metamodels are functionally designed programs to fit a specific set of data. The utilization of metamodels ensures the complete characterization of the system by performing high-end stochastic analysis while keeping the computational cost and time-in check [28–30]. The probabilistic investigations generally struggle to counter the curse of dimensionality. As the system becomes more complex, the curse of dimensionality makes designing the model more critical; other performance issues, such as computational cost and model modification, induce inherent challenges as the system's complexity grows. To mitigate these challenges, the present study incorporates the high-dimensional model representation (HDMR) metamodel to carry out the large-scale MCS-based stochastic investigation of FPF of the laminated composite. HDMR is generally considered for modeling physical problems with a high number of input and output parameters having high-dimensional correlations. The two commonly used HDMRs are random sampling (RS) and cut-HDMR [31]. The functional differences in the RS-HDMR and cut-HDMR can be attributed to the selection of sample points for model construction [31–34]. The utility of HDMR has been in practice in various domains, such as Boussaidi et al. [35] incorporated the RS-HDMR and Gaussian process regression (GPR) to compute the vibration spectra by considering molecular potential energy surfaces. In another study, Chowdhury et al. [36] evaluated the piece-wise continuous function by using the HDMR metamodel to map the partial and total involvement of the input variables with distinct responses. Similarly, Shorter et al. [37] and Miller et al. [38] reported the application of HDMR to assess the correlation between the input and output of the chemical kinematic models from a set of multivariable data in a biological network structure. RS-HDMR belongs to a wider class of methods known as polynomial chaos expansion (PCE) [39], wherein both PCE and RS-HDMR use the orthonormal basis function. The difference in PCE and RS-HDMR lies in evaluating the coefficients. The PCE utilizes the *Stieltjes procedure* [40] to assess the orthonormal polynomial functions, whereas, in the RS-HDMR, we used the *Pearson coefficient index* and *Spearman coefficient index* [47] to evaluate the orthonormal polynomial functions. A few research groups have reported the successful implementation of HDMR metamodel in different domains [41–46]. We utilized the *MATLAB*-based *GUI* of RS-HDMR prepared by Zeihn and Tomlin [47], which is one of the best models to cope with nonlinear datasets with a higher number of input variables. It should be noted that the RS-HDMR directly provides us with model validation parameters such as relative accuracy (RA) and coefficient of correlation (R^2). The model also offers variance-based global sensitivity indices for first-and second-order polynomial functions along with the metamodel validation parameters. To address the inherent challenges of *GUI*, we performed the benchmarking of the RS-HDMR model with a separate Gaussian process regression (GPR) model using the same dataset used for constructing the RS-HDMR model. The prediction capabilities and final responses of both models (RS-HDMR and GPR) are compared in terms of error analysis and sensitivity indices. Subsequently, the distribution of failure loads derived from both models is compared to ensure the predictive accuracy of the RS-HDMR model.

The sensitivity analysis is carried out to determine the relative influence of the input variables on the considered physical phenomenon. The research community frequently utilizes it to establish the importance of the significant parameters in determining the desired responses [48, 49]. For instance, Azadi et al. [50] conducted the sensitivity analysis for carbon/epoxy composite, and they observed that the displacement amplitude is highly sensitive in assessing low-cycle fatigue of the composites. Similarly, Thapa et al. [51] identified the sensitive parameters in progressive failure load analysis by performing the global sensitivity analysis. Tafreshi [52] performed the shape sensitivity analysis to investigate the design of the shapes of an anisotropic material by utilizing the boundary element method. Similarly, throughout a wide range of research disciplines, a few research groups have utilized sensitivity analysis to reveal the critical information of the desired system [53–56]. Due to hefty input variables and low-order parametric correlations, the RS-HDMR expansion used in the stochastic first-ply failure model design is highly useful. Moreover, the RS-HDMR observations are validated with the GPR model observations, which are found to be in good agreement. The scientific contribution of this study is to take layer-wise (8 layers) uncertain material properties into account and conduct a probabilistic investigation to determine the first ply failure load using five different failure criteria, namely maximum strain criterion, maximum stress criterion, Tsai-Hill criterion, Tsai-Wu criterion, and Hoffman criterion. It is noticed from the brief literature review that the role of parametric interactions is scarcely reported in the past while performing the sensitivity analysis. To mitigate this lacuna, we proposed the RS-HDMR-based framework to perform the variance-based sensitivity analysis of the FPF of the eight-layer laminated composite plate in a computationally efficient manner. We compared the deliverables of RS-HDMR with the observations offered by the GPR model to determine the computational accuracy of the proposed RS-HDMR-based sensitivity analysis framework. The current study will aid in the bottom-up design of laminated composites for application-specific deployments.

2 Mathematical formulation

The finite element analysis for the FPF load of a cantilever laminated composite plate is considered in the present study. The governing equation for a multilayered laminated composite is developed from the minimum total potential energy theorem [19], which further allows us to define the structural analysis based on FE modeling. The total potential energy of a body is the summation of total energy due to the body's strain and total work potential due to external forces. The total potential energy can be stated as follows

$$\Pi = U + V \tag{1}$$

The total energy due to strain (U) can be defined as

$$U = \frac{1}{2}\int_{\phi} \{u\}^T\{\sigma\}d\phi \tag{2}$$

The total work potential (V) can be stated as

$$V = \iint_A [u]^T[q]dA \tag{3}$$

$$\{q\} = \{0\ 0\ q_z\ 0\ 0\}^T \tag{4}$$

q_z is the load intensity (transverse). The final stress vector can be expressed as,

$$[F] = [\varepsilon][D] \tag{5}$$

The displacement parameters of the cantilever plate are formulated as

$$\delta_x(x,y,z) = \delta_{x_0}(x,y) - z\theta_x(x,y)\delta_x(x,y) \tag{6}$$

$$\delta_y(x,y,z) = \delta_{y_0}(x,y) - z\theta_y(x,y)\delta_y(x,y) \tag{7}$$

$$\delta_y(x,y,z) = \delta_{z_0}(x,y) = \delta_z(x,y) \tag{8}$$

where δ_x, δ_y, δ_z signify the displacements at the mid-plane, θ_x and θ_y are the rotational components. Stress–strain relation is stated as

$$\begin{aligned}\varepsilon_x &= \frac{\partial\delta_{x_0}}{\delta x} - z\frac{\partial^2\delta_{y_0}}{\delta x^2}, \varepsilon_y = \frac{\partial\delta_{y_0}}{\delta y} - z\frac{\partial^2\delta_{y_0}}{\delta y^2},\\ \gamma_{xy} &= \frac{\partial\delta_{x_0}}{\delta y} + \frac{\partial\delta_{y_0}}{\delta x} - 2\frac{\partial^2\delta_{z_0}}{\delta x\delta y}\end{aligned} \tag{9}$$

The stress–strain relation in the form of a matrix can be formulated as

$$\begin{Bmatrix}\varepsilon_x\\ \varepsilon_y\\ \gamma_{xy}\end{Bmatrix} = \begin{Bmatrix}\varepsilon_x^0\\ \varepsilon_y^0\\ \gamma_{xy}^0\end{Bmatrix} + \begin{Bmatrix}k_x\\ k_y\\ k_{xy}\end{Bmatrix} \tag{10}$$

The force resultant of the lamina can be stated as

$$\{F\} = \left\{\tilde{D}_{xx}\tilde{D}_{yy}\tilde{D}_{xy}\tilde{M}_{xx}\tilde{M}_{xy}\tilde{T}_{xx}\tilde{T}_{yy}^T\right\} \tag{11a}$$

$$\{F\} = \int_{\frac{h}{2}}^{-\frac{h}{2}} \{\sigma_x\sigma_y\tau_{xy}\sigma_x z\sigma_y z\tau_{xy}z\tau_{yz}\tau_{xz}\}^T dz \tag{11b}$$

The stress resultants are as follows

$$(\underset{xx}{\tilde{D}}, \underset{yy}{\tilde{D}}, \underset{xy}{\tilde{D}}) = \int_{-\frac{h}{2}}^{\frac{h}{2}} \{\sigma_x\sigma_y\sigma_{xy}\}dz \tag{12a}$$

$$(\underset{xx}{\tilde{M}}, \underset{yy}{\tilde{M}}, \underset{xy}{\tilde{M}}) = \int_{-\frac{h}{2}}^{\frac{h}{2}} \{\sigma_x\sigma_y\sigma_{xy}\}zdz \tag{12b}$$

$$(\underset{xx}{\tilde{T}}, \underset{yy}{\tilde{T}}) = \int_{-\frac{h}{2}}^{\frac{h}{2}} \{\sigma_{xz}\sigma_{yz}\}zdz \tag{12c}$$

while implementing first-order shear deformation theory (FSDT) using FE-based approach, the variables for displacement and the rotational component are expressed as,

$$u_0(x,y,t:\xi) = \sum_{j=1}^{m} u_j(t:\xi)\psi_j^e(x,y) \tag{13a}$$

$$v_0(x,y,t:\xi) = \sum_{j=1}^{m} v_j(t:\xi)\psi_j^e(x,y) \tag{13b}$$

$$w_0(x,y,t:\xi) = \sum_{j=1}^{m} w_j(t:\xi)\psi_j^e(x,y) \tag{13c}$$

$$\phi_x(x,y,t:\xi) = \sum_{j=1}^{m} S_j^1(t:\xi)\psi_j^e(x,y) \tag{13d}$$

$$\phi_y(x,y,t:\xi) = \sum_{j=1}^{m} S_j^2(t:\xi)\psi_j^e(x,y) \tag{13e}$$

Considering the shape functions (ψ_j^e) of the same order for the entire domain, the generalized equation can be defined as

$$x(\xi,\eta) = \sum_{j=1}^{n} x_j^e\psi_j^e(\xi,\eta) \tag{14}$$

$$y(\xi,\eta) = \sum_{j=1}^{n} y_j^e\psi_j^e(\xi,\eta) \tag{15}$$

Based on FSDT, the displacement and rotational components in Eqs. (13a)–(13e) can be defined as

$$[F^e] = [\{M_e\}\{\underset{e}{\ddot{\Delta}}\} + \{K_e\}\{\Delta^e\}] \tag{16}$$

Finally, the resultant matrix due to transverse shear, stress (in-plane), and moment in terms of $[A]$, $[B]$, and $[D]$ matrix is expressed as

$$[\tilde{T}] = [A]\{y\} \tag{17a}$$

$$[\tilde{D}] = [B]\{k\} + [A]\{\varepsilon^0\} \tag{17b}$$

$$[\tilde{M}] = [D]\{k\} + [B]\{\varepsilon^0\} \tag{17c}$$

The force matrix derived by Eq. (16) is used to determine the first ply failure of the laminated composite plates using different failure criteria. The detailed mathematical understanding of the five failure criteria, viz., maximum strain criterion, maximum stress criterion, Tsai-Hill criterion, Tsai-Wu criterion, and Hoffman criterion is explained in section SM.1 of the *supplementary material*.

2.1 Finite element formulation

The FE modeling is performed for a laminated composite plate by considering an iso-parametric quadratic plate element. Each element comprises eight nodes with five degrees of freedom (DOF), wherein three DOF are translational, and two are rotational. The FE model has mid-surface nodes. An interpolation polynomial function can define the elemental and nodal relation as

$$\overline{u}(\varsigma,\varphi) = P_0 + P_1\varsigma + P_2\varphi + P_3\varsigma^2 + P_4\varsigma\varphi + P_5\varphi^2 + P_6\varsigma^2\varphi + P_7\varsigma\varphi^2 \tag{18}$$

The shape function $\underset{i}{\bar{S}}$ for the FE-based model is stated as

$$\bar{S}_i = 0.25[(1+\varsigma\varsigma_i)(\varsigma\varsigma_i + \varphi\varphi_i - 1)(1+\varphi\varphi_i)] \text{ (for i = 1, 2, 3 and 4)} \tag{19}$$

$$\bar{S}_i = 0.5[(1+\varphi\varphi_i)\,(1+\varsigma^2)] \text{ (for i = 6 and 8)} \tag{20}$$

$$\bar{S}_i = 0.5[(1+\varsigma\varsigma_i)\,(1+\varphi^2)] \text{ (for i = 6 and 8)} \tag{21}$$

The coordinates of ς and φ are presented in Fig. 1.

The efficiency of the shape function is stated as

$$\sum_{i=1}^{8}\bar{S}_i = 1,\ \sum_{i=1}^{8}\frac{\partial\,\bar{S}}{\partial\varphi} = 0,\ \sum_{i=1}^{8}\frac{\partial\,\bar{S}}{\partial\varsigma} = 0 \tag{22}$$

The coordinates of the element at any point are formulated as

$$x = \sum_{i=1}^{8}\bar{S}_i x_i \text{ and } y = \sum_{i=1}^{8}\underset{i}{\bar{S}}y_i \tag{23}$$

The interrelation between the coordinates of displacement and DOF of nodes is stated as

$$u = \sum_{i=1}^{8}\bar{S}_i u_i,\ v = \sum_{i=1}^{8}\underset{i}{\bar{S}}v_i,\ w = \sum_{i=1}^{8}\bar{S}_i w_i,\ \phi_x = \sum_{i=1}^{8}\bar{S}_i\phi_{xi},\quad \text{and}\quad \phi_y = \sum_{i=1}^{8}\bar{S}_i\phi_{yi} \tag{24}$$

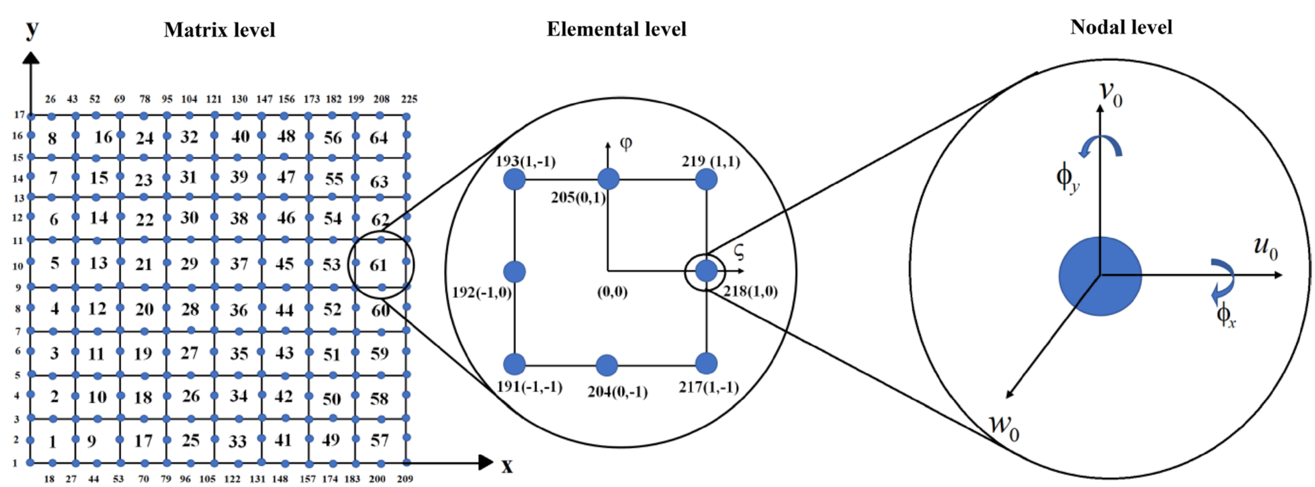

Fig. 1 Coordinate system of the laminate in matrix, elemental and nodal level

The shape function in the form of a Jacobian matrix is stated as

$$\begin{bmatrix} \bar{S}_{i,x} \\ \bar{S}_{i,y} \end{bmatrix} = [J]^{-1} \begin{bmatrix} \bar{S}_{i,\varsigma} \\ \bar{S}_{i,\varphi} \end{bmatrix} \text{ and } [J]^{-1} = \begin{bmatrix} x,\varsigma & x,\varphi \\ y,\varsigma & y,\varphi \end{bmatrix} \tag{25}$$

As it is well established that performing the large-scale (MCS-based) FE simulations renders a huge computational cost, the integration of metamodels such as RS-HDMR and GPR greatly reduces the computational expense and draws a detailed understanding of the failure behavior of the material system. The matrix size-dependent computational cost of conducting FEM simulations is provided in section SM.4 of the *supplementary material*.

Table 1 Range of input parameters under the stochastic effect

Input parameters	Lower bound	Upper bound	Mean
θ (degree)	41.5,−49.5	49.5,−41.5	45,−45
E_1 (Pa)	124×10^9	152×10^9	138×10^9
E_2 (Pa)	8.01×10^9	9.79×10^9	8.96×10^9
G_{12} (Pa)	6.39×10^9	7.81×10^9	7.01×10^9
G_{13} (Pa)	6.39×10^9	7.81×10^9	7.01×10^9
G_{23} (Pa)	2.55×10^9	3.12×10^9	2.84×10^9
μ	0.27	0.33	0.30
$\rho(kg/m^3)$	1440	1760	1600
$t\ (m)$	4.5×10^{-3}	5.5×10^{-3}	5.0×10^{-3}

2.2 Machine learning models

In the present study, we utilized two different machine learning models, random sampling-high-dimensional model representation (RS-HDMR)) and (Gaussian process regression (GPR) to map the failure criteria-specific stochastic first-ply failure load of the laminated composite plates. The methodology adopted to conduct the present study is illustrated in Fig. 2.

In this regard, the eight input parameters (refer to Table 1) are considered for the individual eight layers of the FE model, which lead to the 64 input variables. Each layer has stochastic material properties except for the composite's total thickness (t). Therefore, 64 material parameters are identified, and the total thickness of the material is considered the 65th input variable. The stochasticity in the 65 input variables is enforced by performing random sampling (MCS based), wherein the mean values of the input parameters are perturbed within ± 10% stochastic variation (as per the industry standards). In this way, the random samples are constructed and fed to the FE analysis to calculate the responses in terms of FPF load derived by employing five failure criteria (refer to subsections SM1.1 to 1.5 of *supplementary material*). The dataset generated by the MCS-based FE analysis is used to train and validate

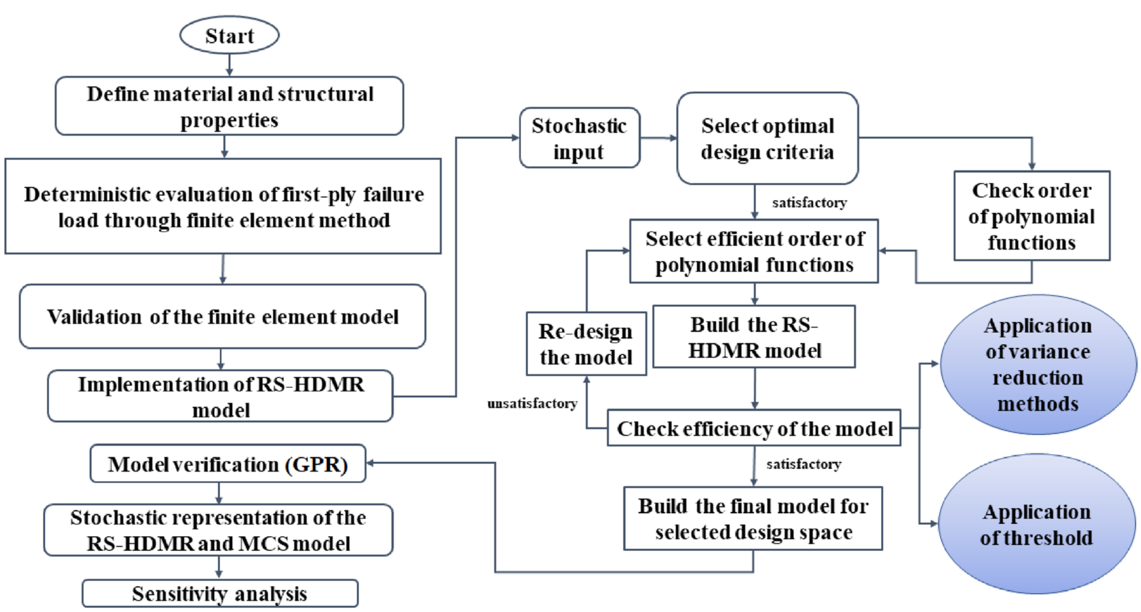

Fig. 2 Algorithm to analyze the stochastic failure analysis incorporating the RS-HDMR approach

the machine learning models considered in the present study.

In the case of RS-HDMR, the convergence study of the appropriate sample size for model construction is performed, wherein the sample size (N_s) for training the model is increased from lower to higher ($N_s = 32$, 64, 128, 256, 512, 1024, and 2048) to check the convergence of sample size which is appropriate for the model construction and results in permissible predictive accuracy. It is to be noted that in the case of RS-HDMR, variance reduction methods are responsible for reducing the error associated with the model. The predictive accuracy of the constructed models is validated by the out-of-fold (separately derived) 2100 samples for which MCS-based FE analysis is performed to evaluate the FPF. A detailed understanding of the mathematical background of the RS-HDMR is provided in section SM.2 of the *supplementary material*. The observations of the RS-HDMR model are compared with the outcomes of the GPR model. The GPR model is constructed with the same 2100 samples where holdout cross-validation is used while training the model. In the holdout cross-validation, at each iteration, N_h (512, 1024, and 2048) samples are held out of the total sample space ($N = 2100$) as the training data, whereas the remaining samples ($N–N_h = 1588$, 1076, and 52) are used to validate the trained model. Such a simultaneous training–testing scheme ensures the sound generalization capability of the model and prevents the model from under-fitting or over-fitting. While training the GPR model, the "*Matern 5/2*" kernel function is utilized by enforcing the isotropic kernel and constant basis function. The detailed mathematical background of the GPR model is presented in section SM.3 of the *supplementary material*.

2.3 Sensitivity analysis

The observations derived from the metamodels (RS-HDMR and GPR) are utilized to perform the sensitivity analysis. The sensitivity analysis offers the relative significance of considered parameters on the desired responses. The variance-based sensitivity analysis is performed for the deliverables of the RS-HDMR model, whereas the relative coefficient of variation-based sensitivity analysis is performed for the deliverables of the GPR model.

2.3.1 RS-HDMR driven variance-based sensitivity analysis

A global variance-based sensitivity analysis is conducted to evaluate the relative significance of the individual input parameters on the FPF of the considered composite plate. A variance-based method [57] is conceptualized in the RS-HDMR model. The partial variances are calculated in the expansion of the output (*refer to subsection SM.2.1 of supplementary material*) to statistically analyze the overall variance for independently distributed random uniform variables.

The total variance (V_t) is obtained by

$$V_t = E(f - f_0) = \sum_i V_{t_i} + \sum_{i<j} V_{t_{ij}} + \ldots + V_{t_{i\ldots n}} \tag{26}$$

The partial variance (V_p) for individual parameters can be obtained by

$$V_p = \int_{[0,1]^l} (f_{i_1\ldots i_l})^2 dx_{i_1} \ldots dx_{i_l} \text{ where } p = i_1, i_2 \ldots i_l \tag{27}$$

The global sensitivity indices [57] can be expressed as

$$S_a = \frac{V_p}{V_t} \tag{28}$$

The variance-based sensitivity analysis utilized in the present model (refer to Fig. 2) is particularly useful for the random input variables. The variance-based sensitivity analysis is carried out for the output function's first- and second-order interactions.

2.3.2 GPR-driven coefficient of variation (CV)-based sensitivity analysis

The coefficient of variation (CV)-based sensitivity analysis is one of the most effective and practiced approaches to define the relative significance of the involved control variables [16, 17, 28, 29]. The individual parametric CV is estimated by normalizing the corresponding standard deviation (s_i) with the mean (m_i) of the response (as shown in Eq. (29)).

$$CV_i = \frac{s_i}{m_i} \tag{29}$$

The total coefficient of variation (TCV) is evaluated as follows-

$$TCV = \sum_{i=1}^{n} CV_i \tag{30}$$

where n denotes the number of control variables ($n = 65$ in the present study). The individual sensitivity indices are obtained by the relative coefficient of variation (RCV), wherein the individual CV's are normalized by TCV as follows-

$$RCV_i = \frac{CV_i}{TCV} \text{where, } \sum_{i=1}^{n} RCV_i = 1 \quad (31)$$

2.4 Model validation

The constructed metamodel is further validated by analyzing the individual model's relative accuracy (RA) and the coefficient of determination (R^2). The formulation of the coefficient of determination [8] is stated as

$$R^2 = 1 - \frac{\sum_{i=1}^{n} (y_i - y_i^{\triangle})^2}{\sum_{i=1}^{n} (y_i - y_i^{-})^2} \quad (32)$$

Here, y_i, and $\overline{y}_i$ signifies the actual model, predicted model, and mean of actual data. In Eq. (33), it is assumed that all the parameters are influential in evaluating the model's efficiency. The relative accuracy of the model [8] is evaluated as

$$RA(\%) = 1 - \left| \frac{J(x)_{\text{predicted}} - J(x)_{\text{actual}}}{J(x)_{\text{predicted}}} \right| \quad (33)$$

$J(x)_{\text{actual}}$ and $J(x)_{predicted}$ are the FE response and corresponding predicted response of the RS-HDMR model, respectively. The current model is designed with 65 input variables. The parameters are chosen based on the number of layers in the laminated composite plate. There are eight layers of the composite with a ply orientation angle $[45°, -45°, 45°, -45°]_s$. Each layer has 8 structural material properties, as stated in Table 1 of the manuscript, which leads to the 64 input parameters. The material's total thickness is considered the 65th input parameter in the present study.

3 Result and discussion

In the present study, an eight-layered laminated composite plate with ply orientation $[45°, -45°, 45°, -45°]_s$ is considered to study the FPF analysis of an AS/3501 graphite-epoxy laminated plate. The material properties utilized to perform the FPF are presented in Table 2.

The present study first reports the MCS-based deterministic observations of the FPF of laminated composite. It is followed by a stochastic investigation using the RS-HDMR and GPR metamodels. Prior to diving deep into the deterministic and stochastic FPF analysis, the responses are validated with the values reported in the previous literature (refer to Tables 3 and 4). The size configuration of the considered plate in the present study is 1 m long,

Table 2 Material properties of carbon-epoxy-based laminated composite plate [58][45°, −45°, 45°]

E_1 (GPa)	E_2 (GPa)	G_{12} (GPa)	G_{13} (GPa)	G_{23} (GPa)	μ	ρ (kg/m^3)
138	8.96	7.10	7.10	2.84	0.30	1600

Table 3 Validation of present FE-based model with previous literature [19]

Mesh size	Comparison	Failure criteria				
		Max. strain	Max. Stress	Tsai-Hill	Tsai-Wu	Hoffman
(2×2)	Reddy and Pandey [19]	2854.40	2947.68	2788.80	2886.72	2850.24
	Present study	2948.47	3061.84	2886.78	2923.72	2904.98
(4×4)	Reddy and Pandey [19]	2164.32	2268.64	1803.84	2218.88	2156.80
	Present study	2486.54	2421.34	1846.86	2031.58	2216.93
(8×8)	Reddy and Pandey [19]	1908.16	1940.48	1530.40	1917.76	1905.76
	Present study	2192.66	2023.53	1641.13	2195.57	2061.86

Table 4 Validation for partially clamped laminated composite plates under concentrated transverse load [59]

Failure theory	$[0°/90°]_s$		$[0_2^0/90°]_s$	
	Kam et al. [59]	Present FEM	Kam et al. [59]	Present FEM
Max. strain	64.94	64.70	108.26	109.10
Max. stress	76.04	75.07	122.86	120.64
Tsai-Hill	64.03	64.70	107.06	109.10
Tsai-Wu	68.30	66.03	112.77	110.64
Hoffman	63.60	64.57	106.45	108.90

1 m wide, and 5 mm thick. The FEM-based deterministic model used in the present analysis is verified and validated [19], 59 in Table 3 and Table 4. The validation of three-layered T300/5208 graphite-epoxy laminate with [45°, −45°, 45°] ply orientation angle is presented in Table 3, whereas Table 4 presents the convergence study for a 4-layered $[0°/90°]_s$ and 6-layered $[0^\circ_2/90°]_s$ laminated composite plate for the present FE model with Kam et al. [59]. The deterministic finite element results are in good agreement with the past published literature [19, 59].

3.1 Stochastic analysis

With adequate confidence corroborated in the present study's responses derived from the FE model, the systematic investigation of the stochastic FPF of the laminated composite plate is carried out in detail. At first, the model construction and validation exercise are reported for both the models (RS-HDMR and GPR) in the following paragraphs. Then the models' capabilities are compared in the latter part of this section.

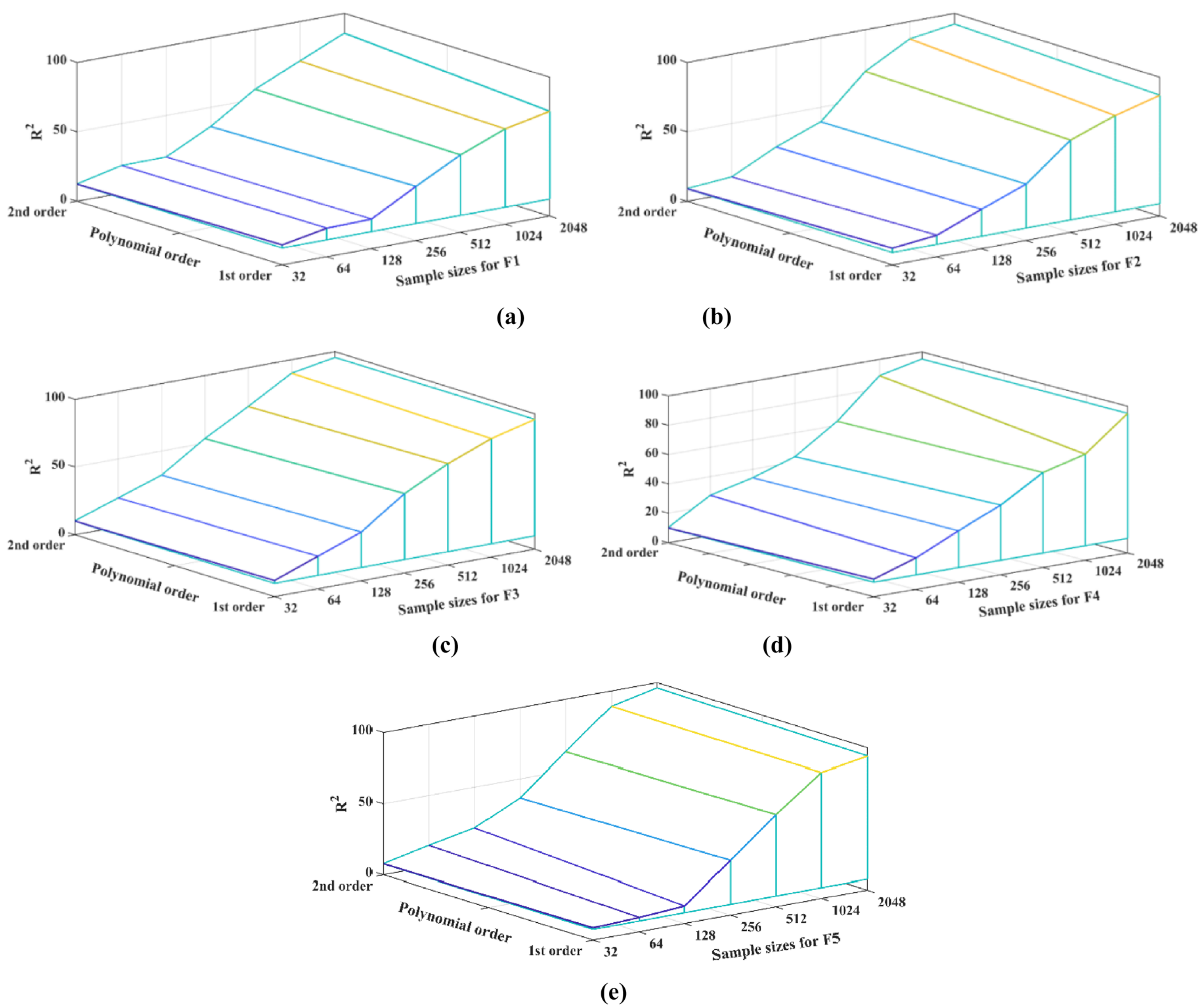

Fig. 3 Coefficient of determination analysis (R^2) for first- and second-order polynomial function with different sample sizes and different failure criteria, viz., **a** Maximum strain criterion (F1), **b** Maximum stress criterion (F2), **c** Tsai-Hill criterion (F3), **d** Tsai-Wu criterion (F4), **e** Hoffman criterion (F5)

3.1.1 RS-HDMR model construction and validation

The RS-HDMR model is constructed by considering the different sizes of sample space (N_s). The goodness of fit of the individual model is assessed by observing the corresponding coefficient of correlation (R^2) value. The comparison of R^2 values of different models (constructed with the differently sized sample spaces, $N_s = 32$, 64, 128, 256, 512, 1024, and 2048) for the individual response is illustrated in Fig. 3. As mentioned earlier, the RS-HDMR model is constructed up to second-order interactions between the input variables. In Fig. 3, a three-dimensional bar graph is illustrated to display the transition of coefficient of correlation (R^2) with respect to first- and second-order polynomial functions corresponding to the different sizes of sample space. The zeroth-order term can be calculated by the mean of output. The x-axis represents the order of the polynomial functions. The y-axis (vertical line) represents the percentage of coefficient of correlation. The z-axis represents the different sample sizes considered to analyze the efficiency of the model. It is observed from the three-dimensional plots furnished in Fig. 3 that as the sample size increases, the R^2 of the models improve proportionally.

It is also evident that the sample space with 2048 samples results in a comparatively efficient model in terms of the R^2 value. Both the first- and second-order component functions are represented in a single figure to identify and observe the trend of the model at varying sampling points. It is perceived that the maximum strain criterion results in a relatively lower R^2 value (however, the R^2 is close to 100%) as compared to the other failure criteria. Despite the promising observations from the comparison of R^2 values, the observations obtained from the RS-HDMR model are further validated by comparing the relative accuracy of the individual models. In this regard, the relative accuracy (RA) in the RS-HDMR-predicted response and FEM-derived response is obtained. The accuracy analysis is performed by considering three different modes, viz., 1%, 5%, and 10%, wherein 1% means that the dataset consists of the MCS-driven perturbation of ± 1% in the mean values of the considered parameters; likewise, the 5% and 10% can be perceived.

Such detailed error analysis not only reveals the predictive capability of the constructed metamodel for the out-of-fold unknown samples but also provides the measure of the uncertainty in the prediction of the responses associated with the practically relevant uncertain variations in the input parameters. The observations drawn from the accuracy analysis are presented in Fig. 4 in the form of three-dimensional bar plots with distinct colors. The relative accuracy and its three modes (1%, 5%, and 10%) are represented in percentage. It is evident from the error analysis (refer to Fig. 4) that for $N_s = 2048$, the relative accuracy is highest for each failure criteria considering the first- and second-order polynomial functions.

3.1.2 GPR model construction and validation

The GPR model is constructed by utilizing the 2100 (N_s) samples constructed by the coupled MCS-based FE analysis. The model is enforced with the holdout cross-validation while training, wherein the N_h ($N_h = 512$, 1024, and 2048) samples are used as the training data at a time, and the remaining samples (N_s-$N_h = 1588$, 1076, and 52) are utilized to validate the constructed model. The goodness of fit and predictive accuracy of the constructed model is assessed by observing the scatter plots and error analysis.

The scatter plots indicate the close-fitting of the GPR model when 2048 samples are used to train the model, and 52 samples are used to validate the model, as illustrated in Fig. 5. It is evident from Fig. 5 that the GPR model shows a promising fit regardless of the responses (F1-F5). In the scatter plot corresponding to F1, the sample points are comparatively much spread (from the linear line) compared to the scatter plots of the other responses, similar to the case of RS-HDMR (which shows less R^2 value). To assess the predictive accuracy of the GPR model, the percentage error in the predicted responses is determined and distributed using the probability density function (pdf) plots depicted in Fig. 6. Figure 6 shows that when the GPR model is trained with 2048 samples, regardless of the responses, the model has a likelihood of minimum (within ± 10%) percentage error in the predictions. The sample size-dependent relative accuracy of the GPR model is compared with the relative accuracy obtained from the RS-HDMR model (refer to Fig. 7). It is evident from Fig. 7 that the relative accuracy of the RS-HDMR is in the vicinity of the GPR model, especially for the case of the models trained with the 2048 samples (refer to Fig. 7c).

This indicates that even though the RS-HDMR model is not cross-validated, it is capable of providing sound predictions. With this understanding, we further compared the deliverables (large-scale predictions) from both models.

3.1.3 Comparison of RS-HDMR with GPR

With the sufficient confidence established by the model verification illustrated in Sects. 3.1.1 and 3.1.2, we further compared the predictions made by both models. In this regard, the randomly distributed 10,000 samples are constructed (with the same ± 10% parametric variation) for which the responses (F1-F5) are predicted by RS-HDMR and GPR model. The comparison of the predicted responses with the

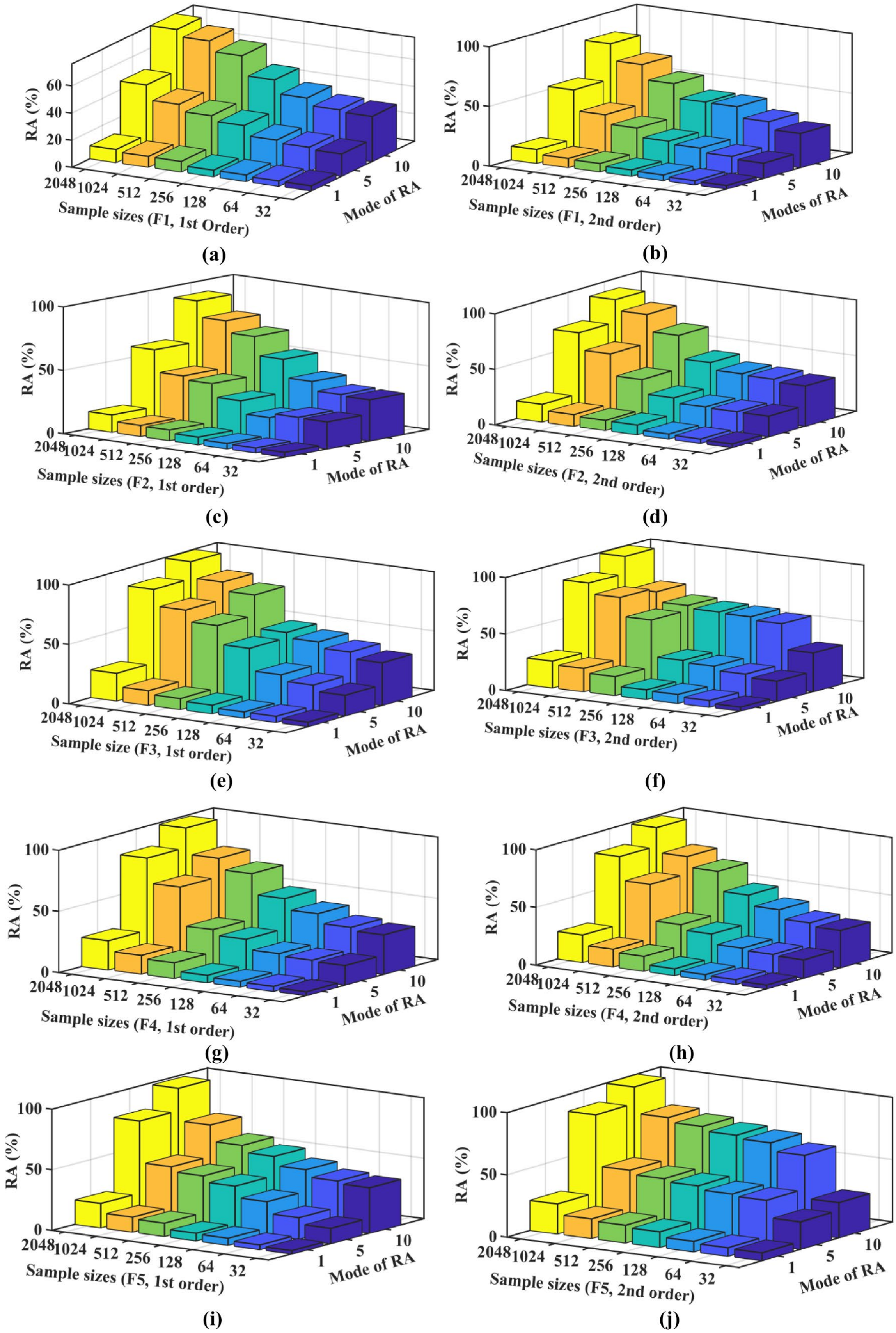
RA (%)
Sample sizes (F1, 1st Order)
Mode of RA
(a)
Sample sizes (F1, 2nd order)
Modes of RA
(b)
Sample sizes (F2, 1st order)
(c)
Sample sizes (F2, 2nd order)
(d)
Sample size (F3, 1st order)
(e)
Sample sizes (F3, 2nd order)
(f)
Sample sizes (F4, 1st order)
(g)
Sample sizes (F4, 2nd order)
(h)
Sample sizes (F5, 1st order)
(i)
Sample sizes (F5, 2nd order)
(j)

◀**Fig. 4** The variation in relative accuracy (RA) of the first-order and second-order function RS-HDMR-predicted FPF by considering different failure criteria (F1-F5) with respect to the change in the sample size

original MCS-based FE outcomes is performed in terms of their probabilistic distribution (refer to Fig. 8).

The pdf of the RS-HDMR and GPR predicted responses almost follows the distribution of the MCS-based FE-driven responses, which indicates that the prediction capabilities of the RS-HDMR and GPR models are comparable. In the next stage, the sensitivity analysis is performed to highlight the relative significance of the individual parameters on the responses. In this regard, the variance-based sensitivity analysis is performed by utilizing RS-HDMR model and relative coefficient of variation (RCV)-based sensitivity analysis is performed by utilizing the GPR model. The detailed mathematical background of both the sensitivity analysis techniques is presented in Sects. 2.4.1 and 2.4.2. The sensitivity indices obtained from both the approaches are compared in Fig. 9. It is worth noting that, despite the functional differences in both approaches (variance-based and relative coefficient of variation (RCV)-based sensitivity analysis), the observations drawn are the same. Figure 9 illustrates that regardless of the failure criteria the highly significant input variables indicated by the variance-based sensitivity analysis are supported by the corresponding sensitivity allocated by the RCV-based sensitivity analysis. It is observed from the sensitivity analysis performed by using both the approaches that the thickness of the laminated plates (x_{65}) is observed to be the most significant parameter regardless of the considered response, also apart from x_{65} majorly higher sensitivity is observed in the ply orientation (x_1-x_8) for all the responses (F1-F5).

The comparison of summation of the first-order sensitivity indices obtained by both the sensitivity approaches (variance-based and relative coefficient of variation (RCV) based sensitivity analysis) is furnished in Table 5. It is observed that the maximum strain criterion results in the highest collective sensitivity index in the case of RCV-based sensitivity analysis, whereas the variance-based sensitivity analysis resulted in the highest collective sensitivity index for the case of Tsai-Hill criterion.

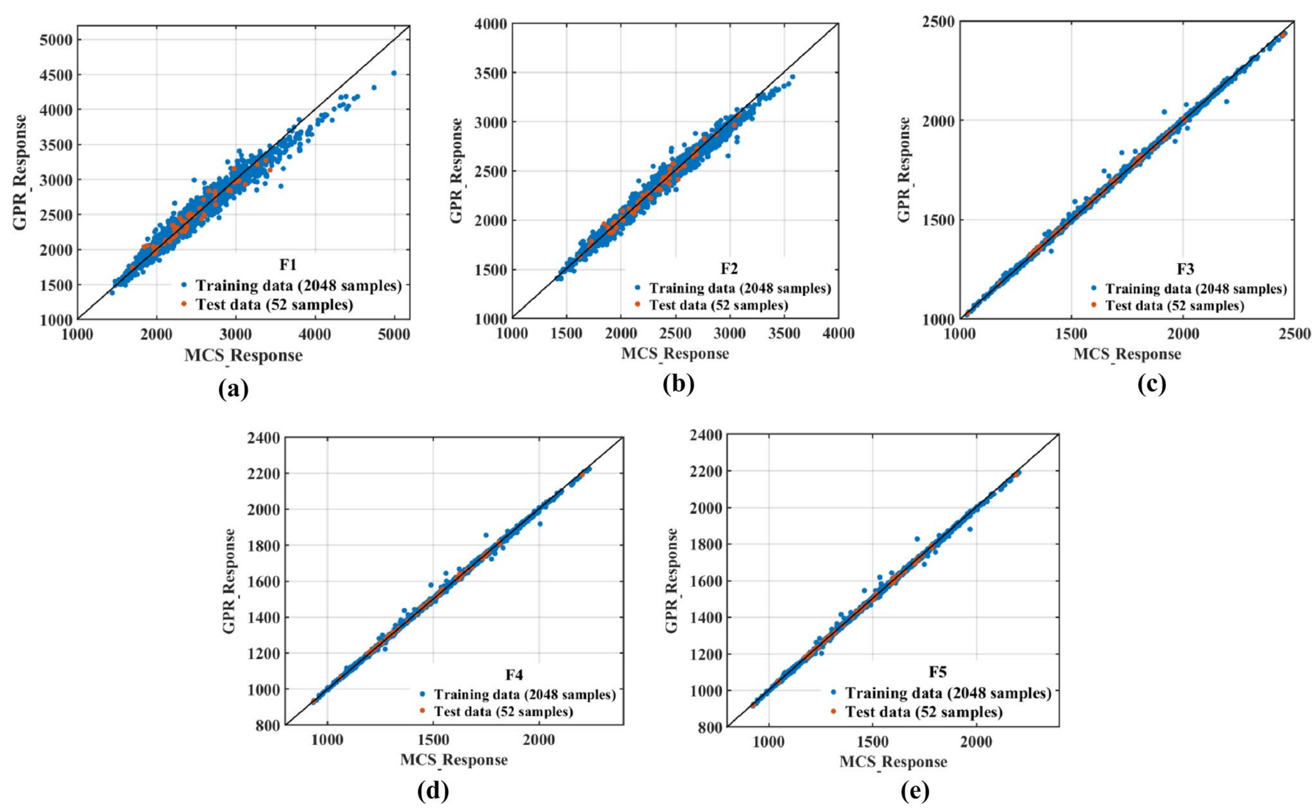

Fig. 5 Scatter plots for training and test data samples against MCS and GPR responses for different failure criteria (F1-F5)

As stated above that despite the total thickness of laminated plates, the ply orientation angles are observed to be relatively the most significant parameters. For instance, the ply orientation angle in the 3rd layer (x_3) is observed as the most significant parameter in obtaining the failure load determined by the maximum strain theory (F1) (refer to Fig. 9a). Similarly, the ply orientation angle for the 8th layer (x_8) dominates other input parameters in determining the failure load by the maximum stress theory (F2), Tsai-Hill theory (F3), Tsai-Wu theory (F4), and Hoffman theory (F5) (refer to Fig. 9b–e).

It is to be noted that the comparison of individual models' verification and their deliverables presented in the preceding paragraphs establishes the computational ingenuity of the responses obtained by the RS-HDMR. With this understanding, further, the second-order polynomial functions of the RS-HDMR model are utilized to perform the prediction for the newly constructed unknown 10,000 samples (as carried out for the analysis shown in Fig. 8). The predictions of second-order polynomial function-based RS-HDMR are compared with original MCS-based FE responses (refer to Fig. 10). Similar to the predictions made by the first-order polynomial function-based RS-HDMR model, the second-order polynomial function also depicts the closeness in the predictions when compared with the distribution of the MCS-based FE responses. The observations drawn from the second-order polynomial function-based sensitivity analysis are presented in Fig. 11, wherein the x- and z-axes represent the two variables contributing simultaneously and the y-axis represents the failure load corresponding to the second-order polynomial function.

Figure 11a–e depicts the plots corresponding to the influence of the two most sensitive parameters on the failure load determined for a particular failure criterion, derived from the second-order polynomial functions-based sensitivity analysis. As an outcome of the second-order polynomial function-based sensitivity analysis, the two most sensitive input parameters are revealed for each case of considered failure

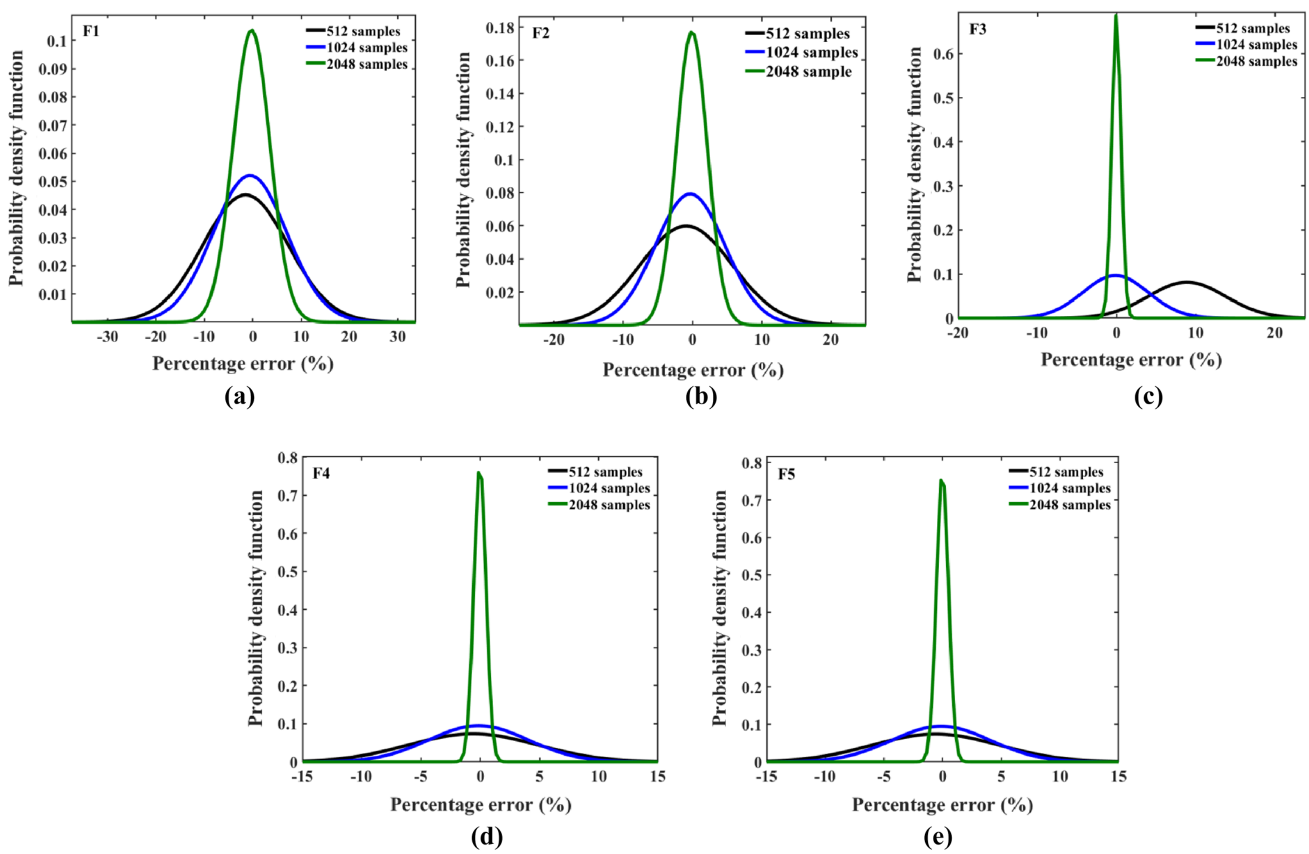

Fig. 6 Error analysis for GPR model for optimum sample sizes for different failure criteria (F1-F5)

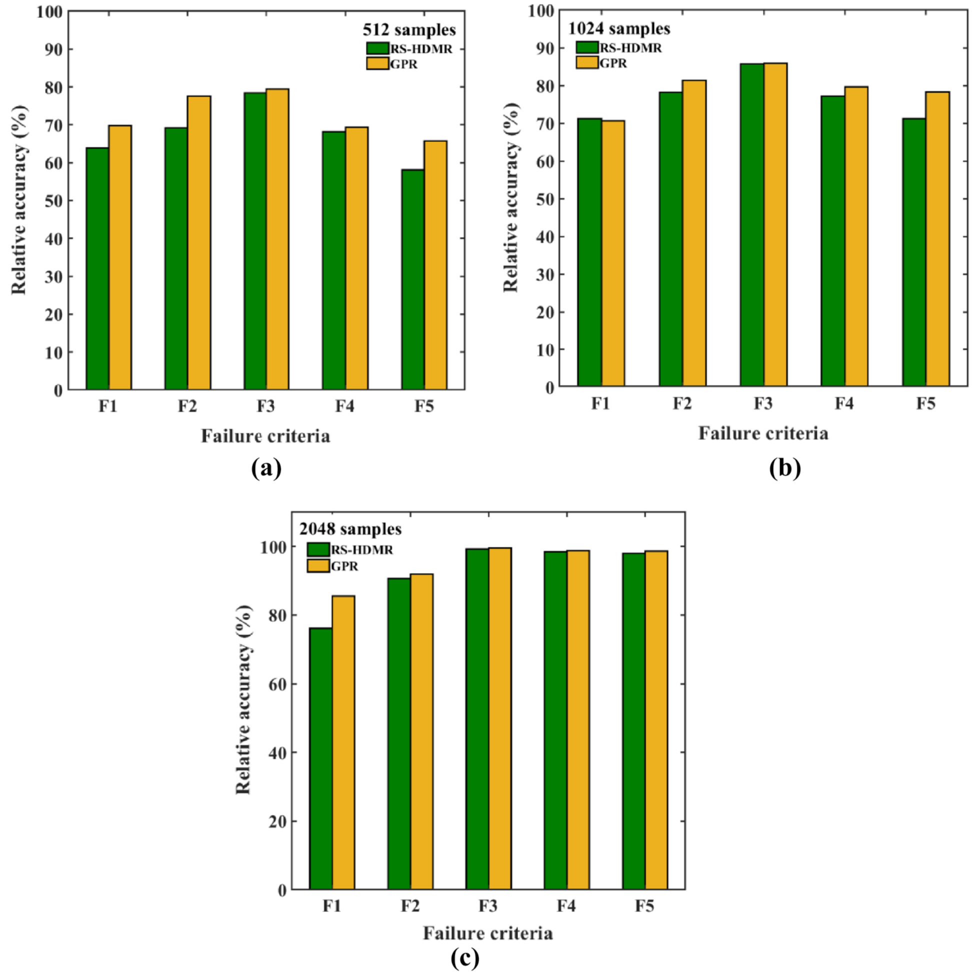

Fig. 7 Relative accuracy analysis for GPR and RS-HDMR model at different sample sizes for different failure criteria (F1-F5)

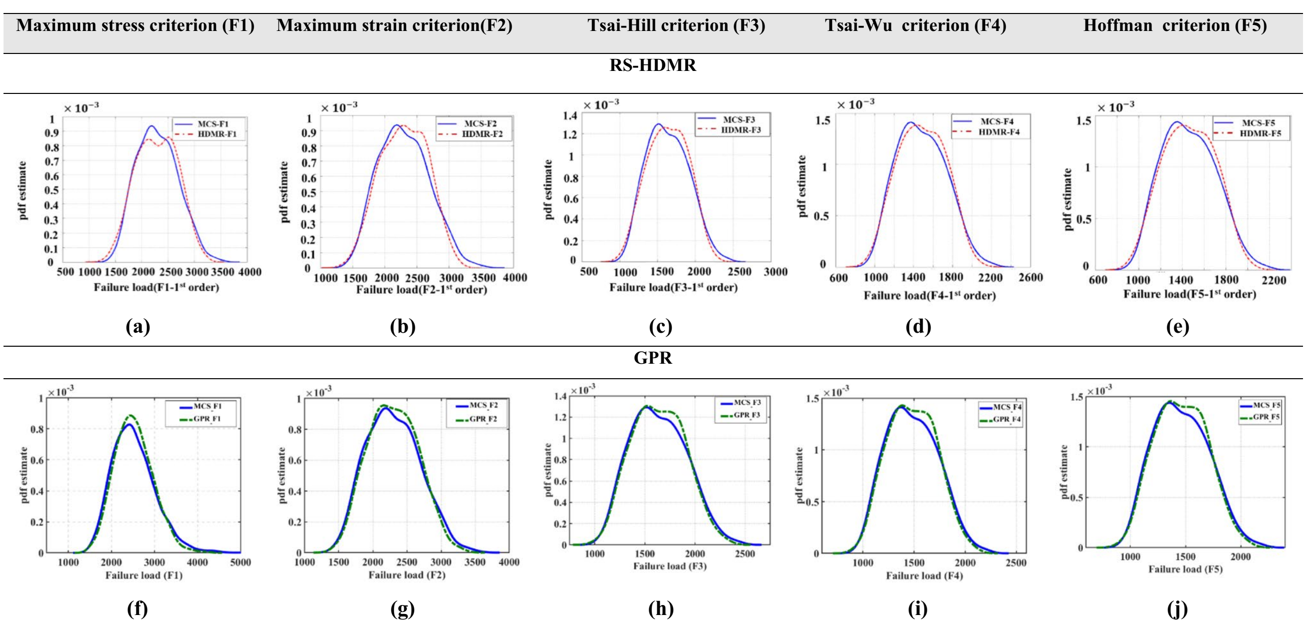

Fig. 8 PDF comparison between RS-HDMR and GPR for 2048 samples for different failure criteria (F1-F5)

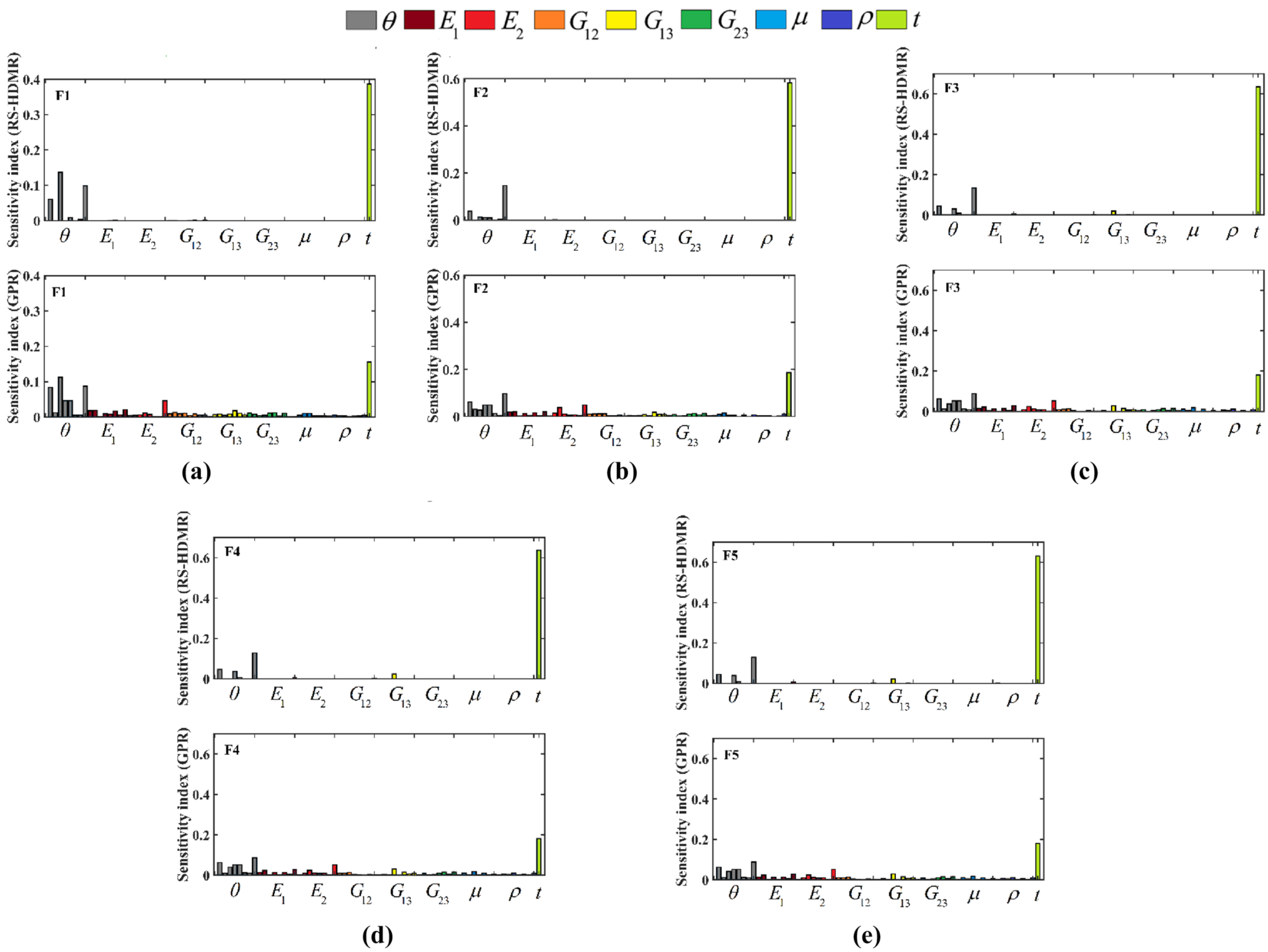

Fig. 9 Sensitivity analysis of input parameters based on RS-HDMR and GPR machine learning models for different failure criteria (F1-F5)

Table 5 Comparison of collective sensitivity index of RCV-based sensitivity analysis (GPR) and variance-based sensitivity analysis (RS-HDMR)

Failure criteria	GPR $TCV = \sum_{i=1}^{n} CV_i$	RS-HDMR $\sum S_i$
Maximum strain criterion	72.52	70.16
Maximum stress criterion	62.00	81.42
Tsai-Hill criterion	66.10	89.12
Tsai-Wu criterion	66.80	88.67
Hoffman criterion	66.77	88.26

criteria. Such as, in the case of the failure load (F1), the ply-orientation angle for the 3rd (x_3) and 4th layer (x_4) has the highest collective sensitivity (refer to Fig. 11a), whereas the ply-orientation angle for 4th layer (x_4) and transverse elastic modulus for 4th layer (x_{20}) dominates while the determination of failure load (F2) (refer to Fig. 11b). Likewise, for failure load (F3), the highest collective sensitivity is found for the transverse elastic modulus of the 3rd layer (x_{19}) and transverse shear modulus of elasticity of the 5th layer (x_{37}) (refer to Fig. 11c). In the case of failure load (F4), the first layer of the transverse shear modulus of elasticity (x_{33}) and Poisson's ratio of the 6th layer (x_{62}) is observed as the most sensitive parameters (refer to Fig. 11d). Lastly, the failure load (F5) is highly influenced by the 6th (x_6) and 8th layer (x_8) of the ply-orientation angle (refer to Fig. 11e).

The sensitivity indices obtained from the first-order polynomial and second-order polynomial functions are compared (for the first five highly ranked variables or variable combinations) for all the responses (F1-F5) in Fig. 12. It is evident from the comparison of sensitivity indices that the first-order terms possess relatively higher sensitivity when compared to the second-order terms.

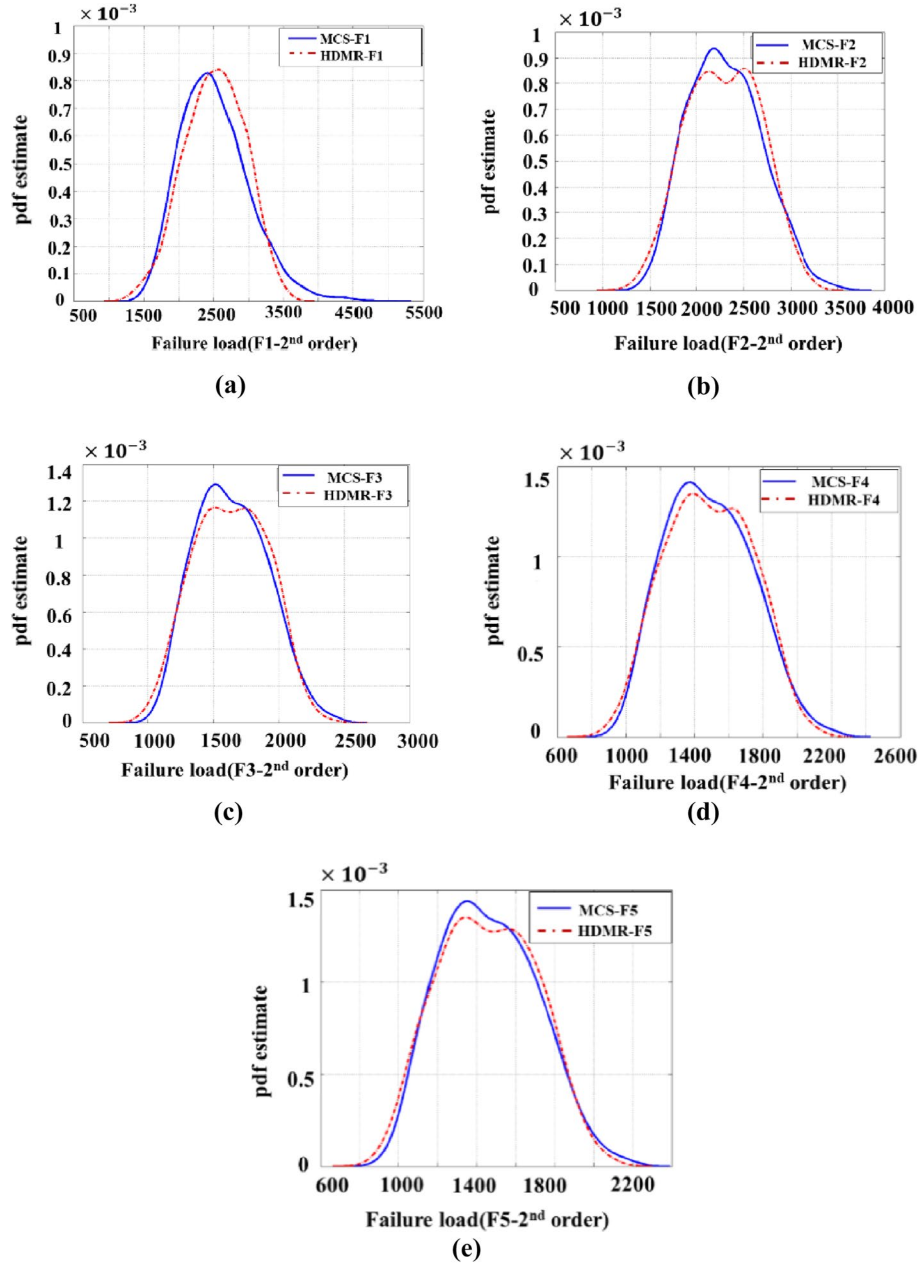

Fig. 10 Pdf for second-order polynomial functions of RS-HDMR and MCS for 2048 samples for five different failure criteria (F1-F5)

4 Conclusions

In the present article, the stochastic first-ply failure load analysis of an eight-layered AS/3501 graphite-epoxy laminated plate with ply orientation $[45°, -45°, 45°, -45°]_s$ is performed by considering five different failure criteria, viz. (a) Maximum strain criterion, (b) Maximum stress criterion, (c) Tsai-Hill criterion, (d) Tsai-Wu criterion, and (e) Hoffman criterion. The eight input parameters (ply-orientation angle, elastic moduli, shear moduli, Poisson ratio, and mass density) are considered for the individual eight layers of the FE model, which leads to the 64 input variables. Along with these 64 input variables, the composite plate's total thickness (t) is randomly varied.

The randomness in the structural and material input properties of the composite plate is introduced by integrating the Monte Carlo simulation (MCS) with the conventional finite element method (FEM) approach. Further, the individual FE models are constructed by enforcing these 65 input conditions to calculate the responses in terms of first-ply failure load by considering the five different failure criteria. The random sampling-high-dimensional model representation (RS-HDMR) model is utilized to conduct the detailed stochastic analysis of the first ply failure of the laminated

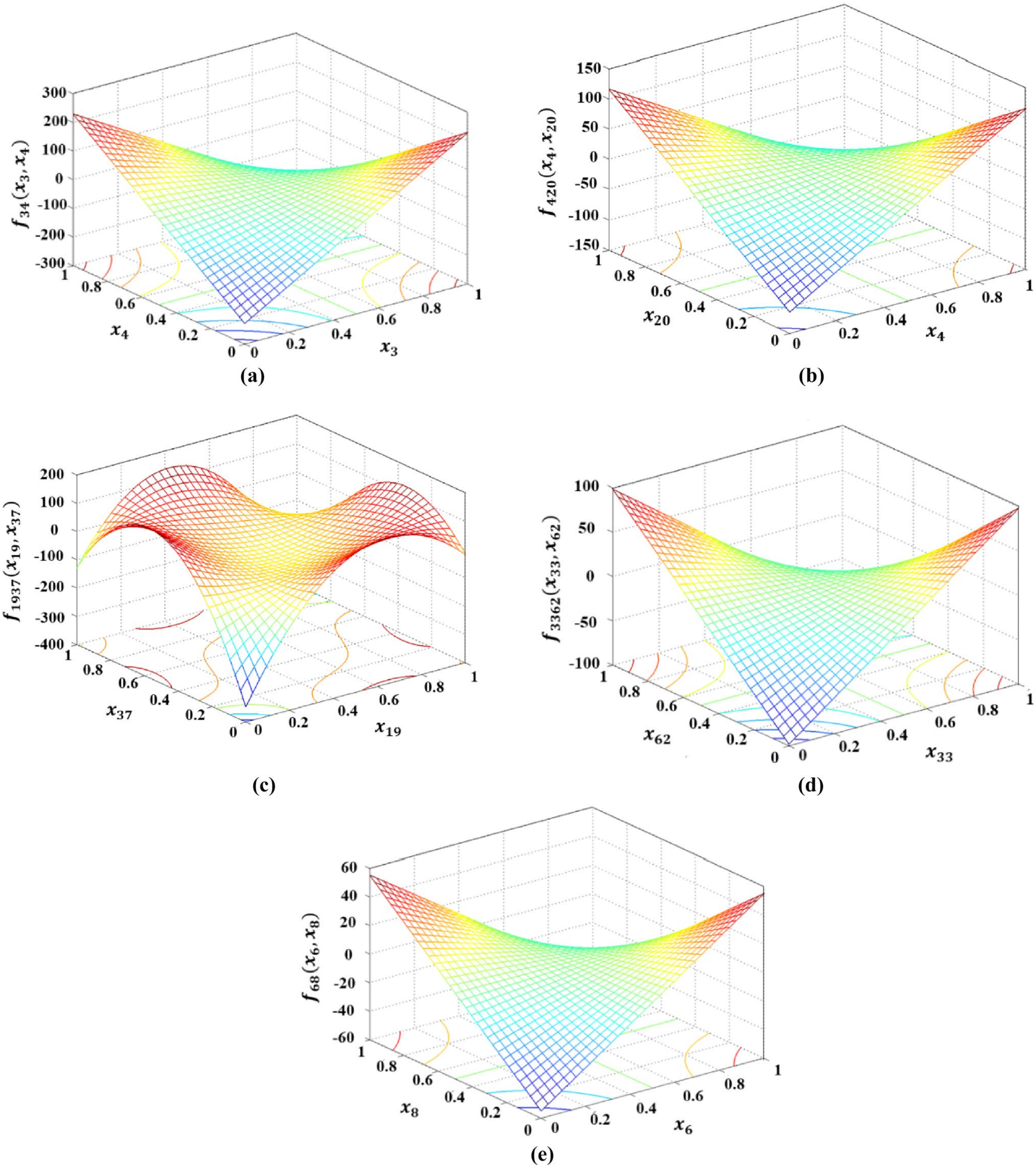

Fig. 11 RS-HDMR component function for variance-based sensitivity analysis for second-order function. **a** the collective influence of x_3 (ply orientation angle for 3rd layer) and x_4 (ply orientation angle for 4th layer) on the failure load determined by maximum strain criterion, **b** collective influence of x_4(ply orientation angle for 4th layer), and x_{20} (transverse elastic modulus for 4th layer) on the failure load determined by maximum stress criterion, **c** collective influence of x_{19} (transverse elastic modulus of 3rd layer) and x_{37} (transverse shear modulus of elasticity of 5th layer) on the failure load determined by Tsai-Hill criterion, **d** collective influence of x_{33} (1st layer of the transverse shear modulus of elasticity) and x_{62} (Poisson's ratio of 6th layer) on the failure load determined by Tsai-Wu criterion, **e** collective influence of the 6th (x_6) and 8th layer (x_8) of the ply-orientation angle on the failure load determined by Hoffman criterion

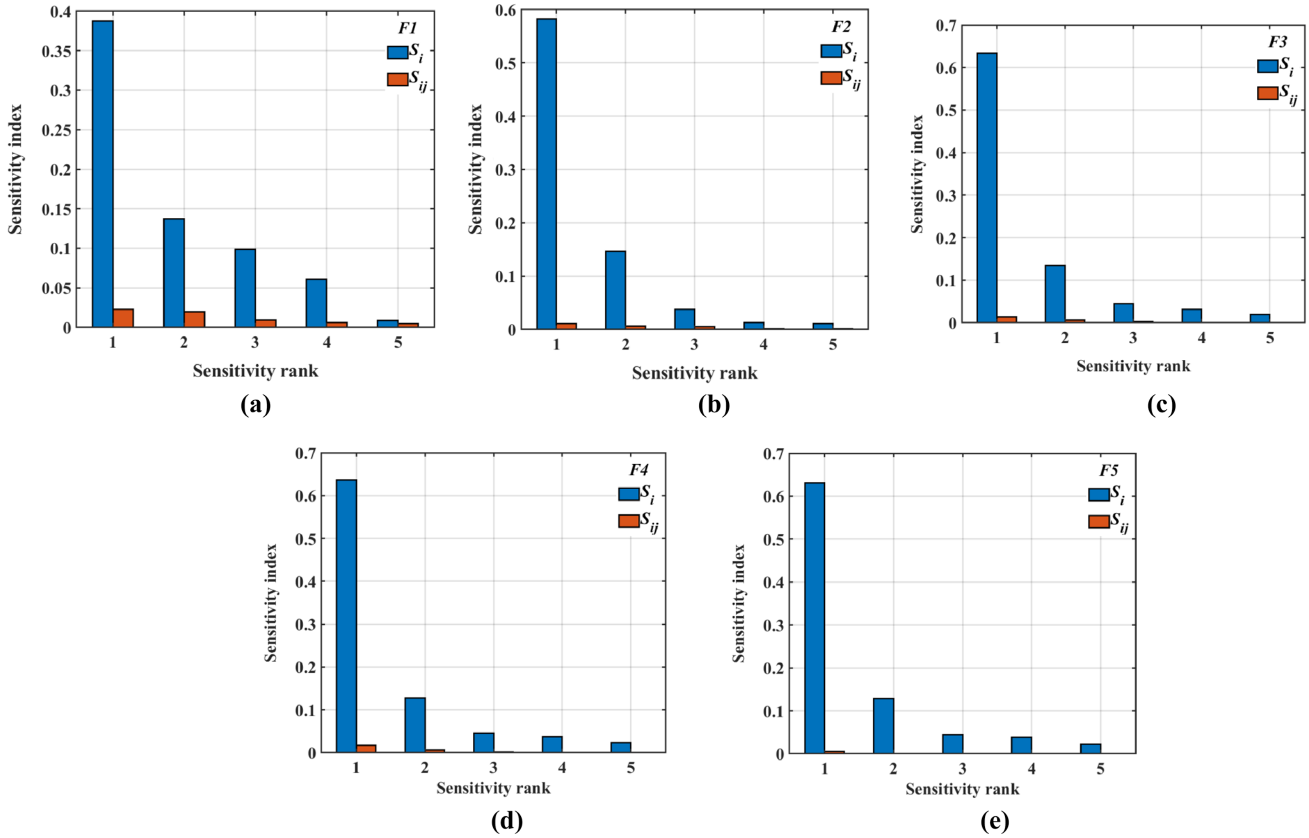

Fig. 12 Comparison of the sensitivity indices obtained from RS-HDMR-driven first-order (S_i) polynomial function and second-order (S_{ij}) polynomial function sensitivity analysis

composite plate. The predictive accuracy of the model is assessed on the basis of the relative accuracy of the predicted responses. We also verified the model's accuracy by comparing the outcomes of the RS-HDMR model with the GPR model.

Such MCS-based metamodeling of the physical problem mitigates the computational expenses associated with the large-scale MCS-based FE models, and at the same time, the constructed models can be used for the in-depth investigation of the material's behavior. With adequate confidence in the developed RS-HDMR model, the model is further deployed to perform the variance-based sensitivity analysis to obtain the relative significance of the considered input parameters. The global sensitivity analysis of the input parameters is performed by using both first- and second-order polynomial functions. It is observed the first-order polynomial functions of the RS-HDMR model dominate the second-order polynomial functions in determining the sensitivity indices. The first-order polynomial functions-based sensitivity analysis revealed that the laminated composite's thickness and ply-orientation angle are the most sensitive parameters in determining the failure load, regardless of the failure criteria utilized. Subsequently, the influence of the two most significant parameters on the failure load derived from the individual failure criteria is investigated by performing the second-order polynomial functions based on sensitivity analysis.

The RS-HDMR model-based framework proposed in the present study demonstrates the successful integration of the MCS, FEM, and RS-HDMR. The exceptional computational efficiency of the developed metamodel reveals deep insights into the first-ply failure of the laminated composite plate, which would otherwise remain unexplored due to the exorbitant nature of performing the large-scale MCS-based FE simulations. The findings of the present study provide critical information about the design paradigm of the laminated composite plate.

Supplementary Information The online version contains supplementary material available at https://doi.org/10.1007/s40430-022-03674-w.

Acknowledgements During this work, the authors gratefully acknowledge the Aeronautics Research and Development Board (Sanction no: ARDB/01/105885/M/I).

Data availability The data that support the findings of this study are available from the authors upon reasonable request.

References

1. Maki LH, Valencia MS, Varoto PS (2021) Dynamic performance and uncertainty analysis of a piezometaelastic structure for vibration control and energy harvesting. Special topics in structural dynamics & experimental techniques. Springer, Cham, pp 215–231. https://doi.org/10.1007/978-3-030-47709-7_21
2. Li S, Benson S (2021) A probabilistic approach to assess the computational uncertainty of ultimate strength of hull girders. Reliab Eng Syst Saf 213:107688. https://doi.org/10.1016/j.ress.2021.107688
3. Paranjape HM, Aycock KI, Bonsignore C, Weaver JD, Craven BA, Duerig TW (2021) A probabilistic approach with built-in uncertainty quantification for the calibration of a superelastic constitutive model from full-field strain data. Comput Mater Sci 192:110357. https://doi.org/10.1016/j.commatsci.2021.110357
4. Red-Horse JR, Benjamin AS (2004) A probabilistic approach to uncertainty quantification with limited information. Reliab Eng Syst Saf 85(1–3):183–190. https://doi.org/10.1016/j.ress.2004.03.011
5. Sun T, Nielsen SR, Basu B (2019) Stochastic control of wave energy converters with constrained displacements for optimal power absorption. Appl Oce Res 89:1–1. https://doi.org/10.1016/j.apor.2019.04.022
6. Zhao MY, Yan WJ, Yuen KV, Beer M (2021) Non-probabilistic uncertainty quantification for dynamic characterization functions using complex ratio interval arithmetic operation of multidimensional parallelepiped model. Mech Syst Signal Process 156:107559. https://doi.org/10.1016/j.ymssp.2020.107559
7. Cao L, Liu J, Xie L, Jiang C, Bi R (2021) Non-probabilistic polygonal convex set model for structural uncertainty quantification. Appl Math Modell 89:504–518. https://doi.org/10.1016/j.apm.2020.07.025
8. Liu J, Yu Z, Zhang D, Liu H, Han X (2021) Multimodal ellipsoid model for non-probabilistic structural uncertainty quantification and propagation. Int J Mech Mater Des. https://doi.org/10.1007/s10999-021-09551-z
9. Hunter MD, Ferche AC, Vecchio FJ (2021) Stochastic finite element analysis of shear-critical concrete structures. ACI Struct J 118(3):71–83. https://doi.org/10.14359/51730524
10. Liu X, Jiang L, Xiang P, Zhou W, Lai Z, Feng Y (2021) Stochastic finite element method based on point estimate and Karhunen-Loéve expansion. Arch Appl Mech 91(4):1257–1271. https://doi.org/10.1007/s00419-020-01819-8
11. Jornet M (2021) Uncertainty quantification for the random viscous Burgers' partial differential equation by using the differential transform method. Nonlinear Anal 209:112340. https://doi.org/10.1016/j.na.2021.112340
12. Li P, Zhang J (2022) Identification and uncertainty quantification of structural flexibility for reliability analysis. Mech Syst Signal Process 163:108104. https://doi.org/10.1016/j.ymssp.2021.108104
13. Kumar RR, Mukhopadhyay T, Naskar S, Pandey KM, Dey S (2019) Stochastic low-velocity impact analysis of sandwich plates including the effects of obliqueness and twist. Thin-Walled Struct 145:106411. https://doi.org/10.1016/j.tws.2019.106411
14. Karsh PK, Kumar RR, Dey S (2019) Stochastic impact responses analysis of functionally graded plates. J Braz Soc Mech Sci Eng 41(11):1–3. https://doi.org/10.1007/s40430-019-2000-8
15. Gupta KK, Mukhopadhyay T, Roy A, Roy L, Dey S (2021) Sparse machine learning assisted deep computational insights on the mechanical properties of graphene with intrinsic defects and doping. J Phys Chem Solids 155:110111
16. Gupta KK, Roy L, Dey S (2022) Hybrid machine-learning-assisted stochastic nano-indentation behaviour of twisted bilayer graphene. J Phys Chemi Solids 167:110711
17. Saha S, Gupta KK, Maity SR, Dey S (2022) Data-driven probabilistic performance of Wire EDM: A machine learning based approach. Proc Instit Mech Eng Part B: J Eng Manuf 236(6–7):908–919
18. Kam TY, Jan TB (1995) First-ply failure analysis of laminated composite plates based on the layerwise linear displacement theory. Compos Struct 32(1–4):583–591. https://doi.org/10.1016/0263-8223(95)00069-0
19. Reddy JN, Pandey AK (1987) A first-ply failure analysis of composite laminates. Comput Struct 25(3):371–393. https://doi.org/10.1016/0045-7949(87)90130-1
20. Onkar AK, Upadhyay CS, Yadav D (2007) Probabilistic failure of laminated composite plates using the stochastic finite element method. Compos Struct 77(1):79–91. https://doi.org/10.1016/j.compstruct.2005.06.006
21. Karsh PK, Mukhopadhyay T, Dey S (2018) Spatial vulnerability analysis for the first ply failure strength of composite laminates including effect of delamination. Compos Struct 184:554–567. https://doi.org/10.1016/j.compstruct.2017.09.078
22. Lal A, Singh BN, Patel D (2012) Stochastic nonlinear failure analysis of laminated composite plates under compressive transverse loading. Compos Struct 94(3):1211–1223. https://doi.org/10.1016/j.compstruct.2011.11.018
23. Martinez JR, Bishay PL (2021) On the stochastic first-ply failure analysis of laminated composite plates under in-plane tensile loading. Compos Part C: Open Access 4:100102. https://doi.org/10.1016/j.jcomc.2020.100102
24. Gadade AM, Lal A, Singh BN (2016) Stochastic progressive failure analysis of laminated composite plates using Puck's failure criteria. Mech Adv Mater Struct 23(7):739–757
25. Mooney CZ. Monte carlo simulation. Sage; (1997) Apr 7.
26. Kushari S, Chakraborty A, Mukhyopadhyay T, Ranjan Kumar R, Ranjan Maity S, Dey S (2021) Surrogate model validation and verification for random failure analyses of composites. Recent advances in layered materials and structures. Springer, Singapore, pp 331–352
27. Kushari S, Chakraborty A, Mukhopadhyay T, Maity SR, Dey S (2021) ANN-based random first-ply failure analyses of laminated composite plates. Recent advances in computational mechanics and simulations. Springer, Singapore, pp 131–142. https://doi.org/10.1007/978-981-15-8138-0_11
28. Gupta KK, Mukhopadhyay T, Roy L, Dey S (2022) Hybrid machine-learning-assisted quantification of the compound internal and external uncertainties of graphene: towards inclusive analysis and design. Mater Adv. https://doi.org/10.1039/D1MA00880C
29. Mukhopadhyay T, Naskar S, Gupta KK, Kumar R, Dey S, Adhikari S (2021) Probing the stochastic dynamics of coronaviruses: Machine learning assisted deep computational insights with exploitable dimensions. Adv Theory Sim 4(7):2000291
30. Mukhopadhyay T, Karsh PK, Basu B, Dey S (2020) Machine learning based stochastic dynamic analysis of functionally graded shells. Compos Struct 237:111870. https://doi.org/10.1016/j.compstruct.2020.111870
31. Li G, Rosenthal C, Rabitz H (2001) High dimensional model representations. J Phys Chem A 105(33):7765–7777. https://doi.org/10.1021/jp010450t
32. Li E, Wang H, Li G (2012) High dimensional model representation (HDMR) coupled intelligent sampling strategy for nonlinear

problems. Comput Phys Commun 183(9):1947–1955. https://doi.org/10.1016/j.cpc.2012.04.017
33. Eftekhari, A. and Scheidegger, S., (2022) High-Dimensional Dynamic Stochastic Model Representation. arXiv preprint arXiv:2202.06555.
34. Li G, Wang SW, Rosenthal C, Rabitz H (2001) High dimensional model representations generated from low dimensional data samples I. mp-Cut-HDMR. J Math Chem 30(1):1–30. https://doi.org/10.1023/A:1013172329778
35. Boussaidi MA, Ren O, Voytsekhovsky D, Manzhos S (2020) Random sampling high dimensional model representation gaussian process regression (RS-HDMR-GPR) for multivariate function representation: application to molecular potential energy surfaces. J Phys Chem A 124(37):7598–7607. https://doi.org/10.1021/acs.jpca.0c05935
36. Chowdhury R, Rao BN, Prasad AM (2008) High dimensional model representation for piece-wise continuous function approximation. Commun Numer Methods Eng 24(12):1587–1609
37. Shorter JA, Ip PC, Rabitz HA (1999) An efficient chemical kinetics solver using high dimensional model representation. J Phys Chem A 103(36):7192–7198. https://doi.org/10.1021/jp9843398
38. Miller MA, Feng XJ, Li G, Rabitz HA (2012) Identifying biological network structure, predicting network behavior, and classifying network state with high dimensional model representation (HDMR). PLoS ONE 7(6):e37664. https://doi.org/10.1371/journal.pone.0037664
39. Zuniga MM, Kucherenko S, Shah N (2013) Metamodelling with independent and dependent inputs. Comput Phys Commun 184(6):1570–1580
40. Jakeman JD, Franzelin F, Narayan A, Eldred M, Plfüger D (2019) Polynomial chaos expansions for dependent random variables. Comput Methods Appl Mech Eng 351:643–666
41. Li G, Hu J, Wang SW, Georgopoulos PG, Schoendorf J, Rabitz H (2006) Random sampling-high dimensional model representation (RS-HDMR) and orthogonality of its different order component functions. J Phys Chem A 110(7):2474–2485. https://doi.org/10.1021/jp054148m
42. Manzhos S, Carrington T Jr (2006) A random-sampling high dimensional model representation neural network for building potential energy surfaces. J Chem Phys 125(8):084109. https://doi.org/10.1063/1.2336223
43. Remacle JF, Lambrechts J, Seny B, Marchandise E, Johnen A, Geuzainet C (2012) Blossom-Quad: a non-uniform quadrilateral mesh generator using a minimum-cost perfect-matching algorithm. Int J Numer Methods Eng 89(9):1102–1119. https://doi.org/10.1002/nme.3279
44. Chowdhury R, Adhikari S (2010) High dimensional model representation for stochastic finite element analysis. Appl Math Modell 34(12):3917–3932. https://doi.org/10.1016/j.apm.2010.04.004
45. Adhikari S, Chowdhury R, Friswell MI (2011) High dimensional model representation method for fuzzy structural dynamics. J Sound Vib 330(7):1516–1529. https://doi.org/10.1016/j.jsv.2010.10.010
46. Rathi AK, Chakraborty A (2021) Improved moving least square-based multiple dimension decomposition (MDD) technique for structural reliability analysis. Int J Comput Methods 18(01):2050024
47. Ziehn T, Tomlin AS (2009) GUI-HDMR - A Software Tool for Global Sensitivity Analysis of Complex Models. Environ Model Softw. https://doi.org/10.1016/j.envsoft.2008.12.002
48. Yaghoubi V, Silani M, Zolfaghari H, Jamshidian M, Rabczuk T (2020) Nonlinear interphase effects on plastic hardening of nylon 6/clay nanocomposites: a computational stochastic analysis. J Compos Mater 54(6):753–763. https://doi.org/10.1177/0021998319868523
49. Kushari S, Mukhopadhyay T, Chakraborty A, Maity SR, Dey S (2022) Probability-based unified sensitivity analysis for multi-objective performances of composite laminates: A surrogate-assisted approach. Compos Struct. https://doi.org/10.1016/j.compstruct.2022.115559
50. Azadi M, Alizadeh M, Sayar H. Sensitivity analysis for effects of displacement amplitude and loading frequency on low-cycle fatigue lifetime in carbon/epoxy laminated composites. In: MATEC Web of Conferences 2018 (Vol. 165, p. 22021). EDP Sciences.https://doi.org/10.1051/matecconf/201816522021
51. Thapa M, Paudel A, Mulani SB, Walters RW (2021) Uncertainty quantification and global sensitivity analysis for progressive failure of fiber-reinforced composites. Struct Multidiscip Opt 63(1):245–265. https://doi.org/10.1007/s00158-020-02690-5
52. Tafreshi A (2009) Shape sensitivity analysis of composites in contact using the boundary element method. Eng Anal Bound Elements 33(2):215–224. https://doi.org/10.1016/j.enganabound.2008.04.008
53. Amor N, Noman MT, Petru M, Mahmood A, Ismail A (2021) Neural network-crow search model for the prediction of functional properties of nano TiO2 coated cotton composites. Sci Rep 11(1):1–3. https://doi.org/10.1038/s41598-021-93108-9
54. Jesthi DK, Nayak RK (2020) Sensitivity analysis of abrasive air-jet machining parameters on machinability of carbon and glass fiber reinforced hybrid composites. Mater Today Commun 1(25):101624. https://doi.org/10.1016/j.mtcomm.2020.101624
55. Kamiński M (2003) Sensitivity analysis of homogenized characteristics for some elastic composites. Comput Methods Appl Mech Eng 192(16–18):1973–2005. https://doi.org/10.1016/S0045-7825(03)00214-7
56. Norenberg JP, Cunha Jr A, da Silva S, Varoto PS. (2020) An application of the global sensitivity analysis on a bistable energy harvester. In: 3rd International conference on engineering vibration (ICoEV 2020) Dec 14.
57. Ziehn T, Tomlin AS (2008) Global sensitivity analysis of a 3D street canyon model—Part I: The development of high dimensional model representations. Atmosp Environ 42(8):1857–1873. https://doi.org/10.1016/j.atmosenv.2007.11.018
58. Kollar LP, (2003) Springer GS. Mechanics of composite structures. Cambridge university press Feb 17.
59. Kam TY, Sher HF, Chao TN, Chang RR (1996) Predictions of deflection and first-ply failure load of thin laminated composite plates via the finite element approach. Int J Solids Struct 33(3):375–398. https://doi.org/10.1016/0020-7683(95)00042-9